Montana State Physics REU Program
Solar Soft X-ray Irradiance With Yohkoh/SXT

1. Introduction

Soft X-ray (SXR) irradiance is defined as the output of light energy per unit area from the Sun as measured by Earth in the form of soft X-rays. ("Solar Irradiance," 2008) SXR irradiance emitted from the Sun constantly affects life on Earth. It is responsible for a wide range of phenomena, such as Transatlantic Radio Communication. Radio waves, which naturally travel in straight lines, cannot pass through solid earth and therefore depend upon a source to reflect them around the curvature of Earth. SXR irradiance produces enough energy to strip atoms of their electrons, creating the ionosphere, which makes the curvature of radio waves possible. (Lang, 2001) In addition, SXR variability impacts atmospheric density and thus satellite drag. At solar maximum, the Sun adds more energy to the atmosphere, and air density at low earth orbit increases. As a result, the atmospheric drag is stronger. The reverse occurs during solar minimum, and measurements of SXR irradiance allow us to adjust orbit calculations accordingly. ("Satellite Drag," 2018) For this particular study, the main goal is to attain knowledge since Yohkoh data is from 1991 to 2001, but understanding the past is critical for analyzing the present.

Yohkoh Soft X-ray Telescope (SXT) data from the 1990s has recently been recalibrated, and information extracted from this data offers insight into the mysteries of astronomy. Yohkoh, along with the *Solar Radiation and Climate Experiment* (SORCE) and the *Geostationary Operational Environmental Satellite Program* (GOES), focuses on the Sun because it is logistically easier to study than farther stars, and it impacts us the most directly. However, studying the Sun and its magnetic variability gives us an understanding of the processes of other stars.

This study focuses on the soft X-ray range of the electromagnetic spectrum in order to analyze radiation at shorter wavelengths, especially at the low corona. Extremely hot material generally emits energy at ultraviolet (UV) and X-ray wavelengths, but the photosphere is too cool to emit this radiation. This is used to our advantage because SXT filters make it possible for us to isolate the corona.

The five filters of Yohkoh SXT, which modify the composite spectral sensitivity of the telescope, include a 1265 Å Al filter and a 2930 Å Al, 2070 Å Mg, 562 Å Mn, and 190 Å C filter. ()
Originally, the effective area (cm^2) was measured between 0 and 30 Å, but later findings deemed 3 to 45 Å the ideal wavelength range. () This study uses Level 2 images from the Yohkoh Legacy Archive (YLA), which are SXT composite images consisting of 2 or 3 long and short exposures to increase dynamic range and remove detector saturation. Level 2 images only include complete or nearly-complete images, and the files are organized by date. ("Data Description," 2010)

The beginning steps of the study included preparing the images, masking the images with certain solar radii to remove contributions from background noise (see Figure 3), and collecting intensity for both the 1265 Å Al and 2930 Å Al, 2070 Å Mg, 562 Å Mn, and 190 Å C filters. Once the intensity was collected, it was converted to temperature (K) and emission measure (cm^{-3}) using the Filter Ratio Method, and subsequently converted to irradiance (W/m^2) using the CHIANTI atomic database. The powerful imaging abilities of Yohkoh SXT, unlike those of other satellites with only full sun detectors, allow analyzation of the hemispheres, as well as specific areas of the Sun, individually.

After calculating the intensity of the images using the data number, the Filter Ratio Method (FRM) was applied. FRM techniques follow the assumption that the Sun has isothermal plasma. Combining the data number (DN) equation, energy of photons (E_i) equation, volume emission measure (E) equation, and response function results in the Ratio equation. (Hara, et al., 1992) Previously, the Ratio equation did not take the Yohkoh SXT prefilter nor telescope damage into consideration. However, it was adjusted to account for carbon buildup on the filters that began after Yohkoh was launched and for punctures in the pre-filter that started to occur during November of 1992 (see comparison in Figure 2).

The temperature and emission measure found from FRM calculations were then analyzed by the CHIANTI atomic database, which takes advantage of atomic data, as well as programs written in Interactive Data Language (IDL) and Python, to evaluate the spectra from astrophysical plasmas. (Dere, et al., 1997) Total coronal irradiance is found by integrating the coronal isothermal spectra, consisting of both the continuum and spikes in the curve, and using the CHIANTI isothermal procedure in tandem with IDL programs. The spikes are emission lines emitted from ionized elements at specific wavelengths, and the CHIANTI atomic database allows us to account for the radiation of these elements. IDL programs also enable wavelength bins to be specified. In the beginning of this study, wavelengths of 0 to 30 Å were used, but this was changed to 3 to 45 Å because Yohkoh SXT is more precise at these wavelengths. All graphs have a 3 to 45 Å range unless otherwise stated (see Figure 1).

Different types of data analysis were performed to better comprehend the information provided by Yohkoh SXT. Some of the data analysis is shown by the graphs in Figures 1 through 6. Experiments include comparing old and new FRM calibrations, adjusting the masked radius, removing faulty images, and calculating irradiance pixel-by-pixel. All graphs measure 1.2 solar radii unless otherwise stated. Along with, and occasionally instead of, graphs showing 1991 through 2001, graphs depicting only 1992 are shown. The graphs of only 1992 serve to increase visual clarity and to better portray variability between months. 1992 was chosen as the example year because data from earlier years are more reliable since carbon buildup and punctures in the filters were minimal. Yohkoh launched on August 30th, 1991, so a full data set for 1991 does not exist, and therefore 1992 was used.

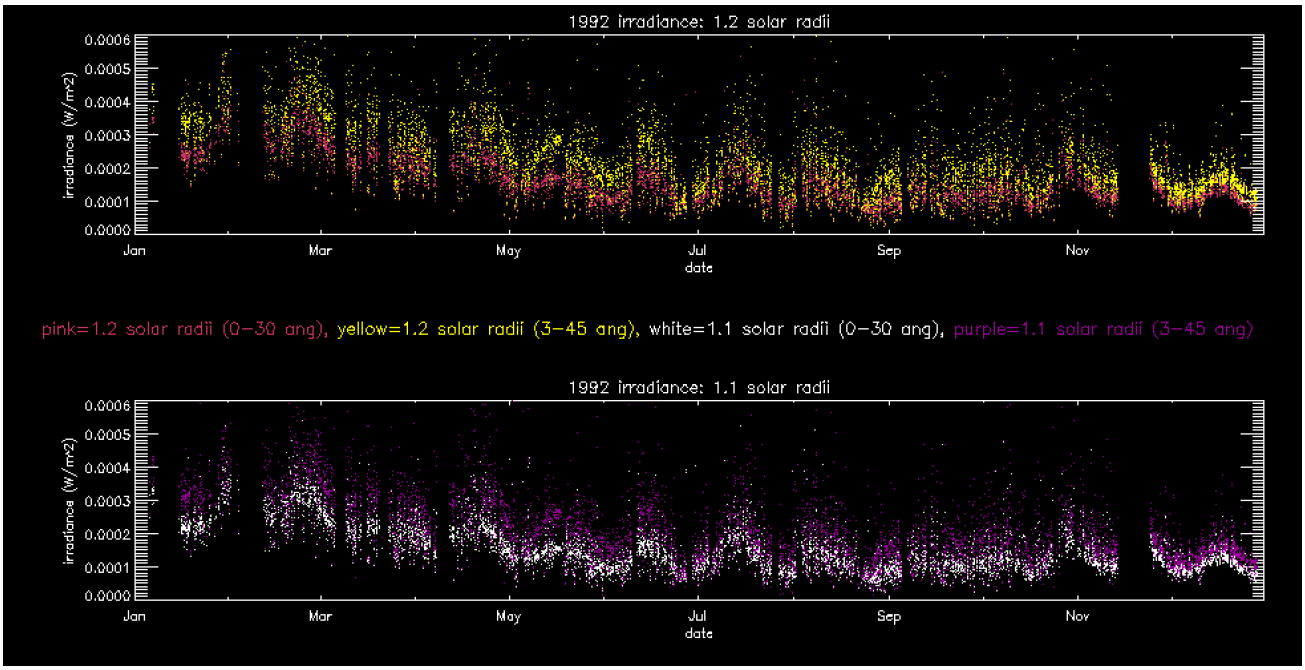

Figure 1. These graphs show how different wavelength ranges affect the total irradiance measure for masked images of 1.1 radii and 1.2 radii. Both graphs show 1992. The top graph is the total irradiance with a mask of 1.2 solar radii. Pink is 1.2 solar radii with a 0-30 Å range and yellow is 1.2 solar radii with 3-45 Å range. The bottom graph is the total irradiance with a mask of 1.1 solar radii. White is 1.1 solar radii with a 0-30 Å range and purple is 1.1 solar radii with a 3-45 Å range.

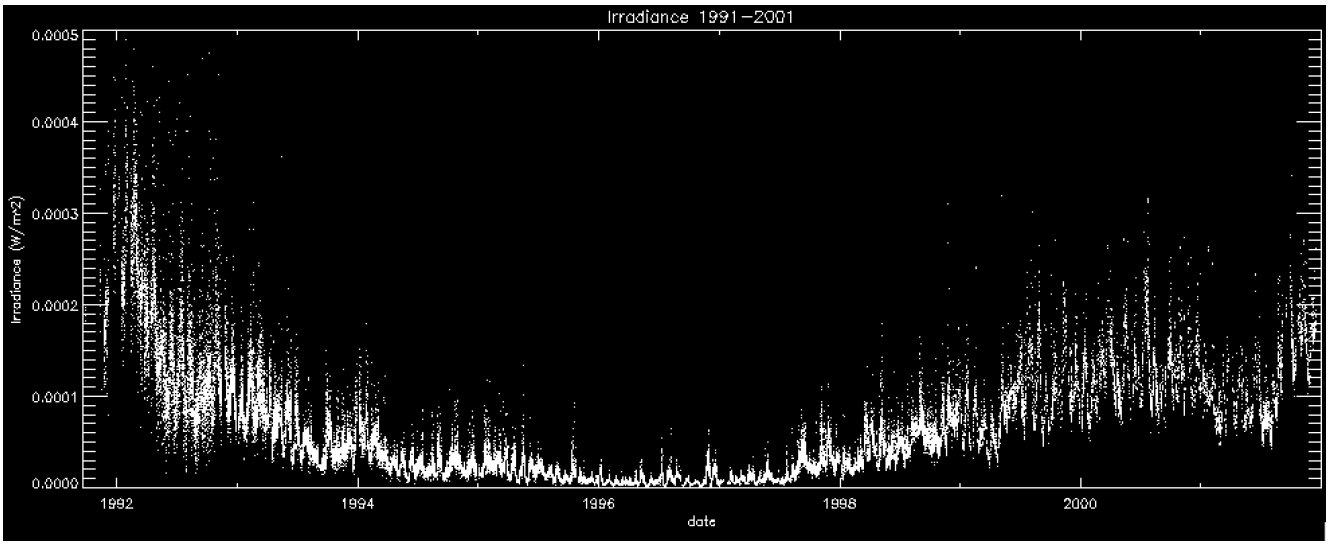

Total irradiance 1991-2001 3-45 ang, 1.1 radii. Note x-axis max is .0005 W/m^2. (Graphs should include both wbins.)

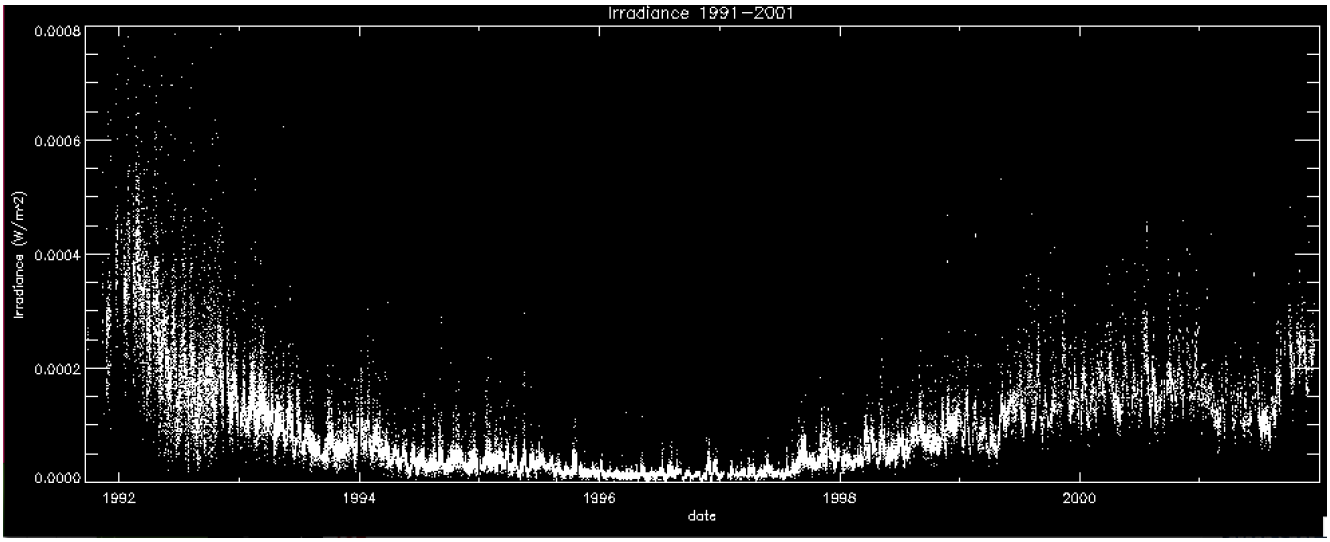

Total irradiance 1991-2001. 3-45 ang, 1.2 radii. Note x-axis max is .0008 W/m^2. (Graphs should include both wbins.)

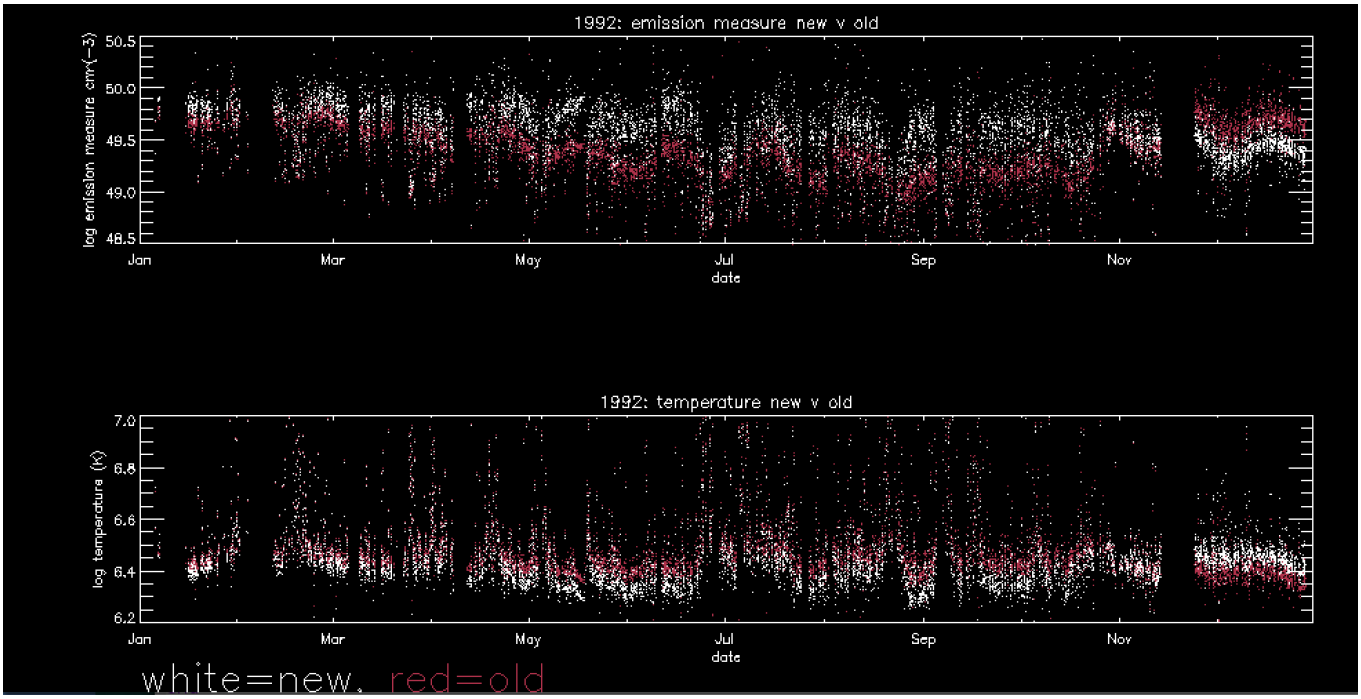

Figure 2. These graphs show the difference in temperature and emission measure in 1992 when using the original and updated FRM equations. The top graph shows emission measure, where white is the updated FRM equation and red is the original FRM equation.
The updated FRM equation accounts for carbon buildup and punctures in the filters. After November of 1992, Yohkoh was unable to produce more visible light images. Fortunately, X-ray images were produced but affected by the punctures.

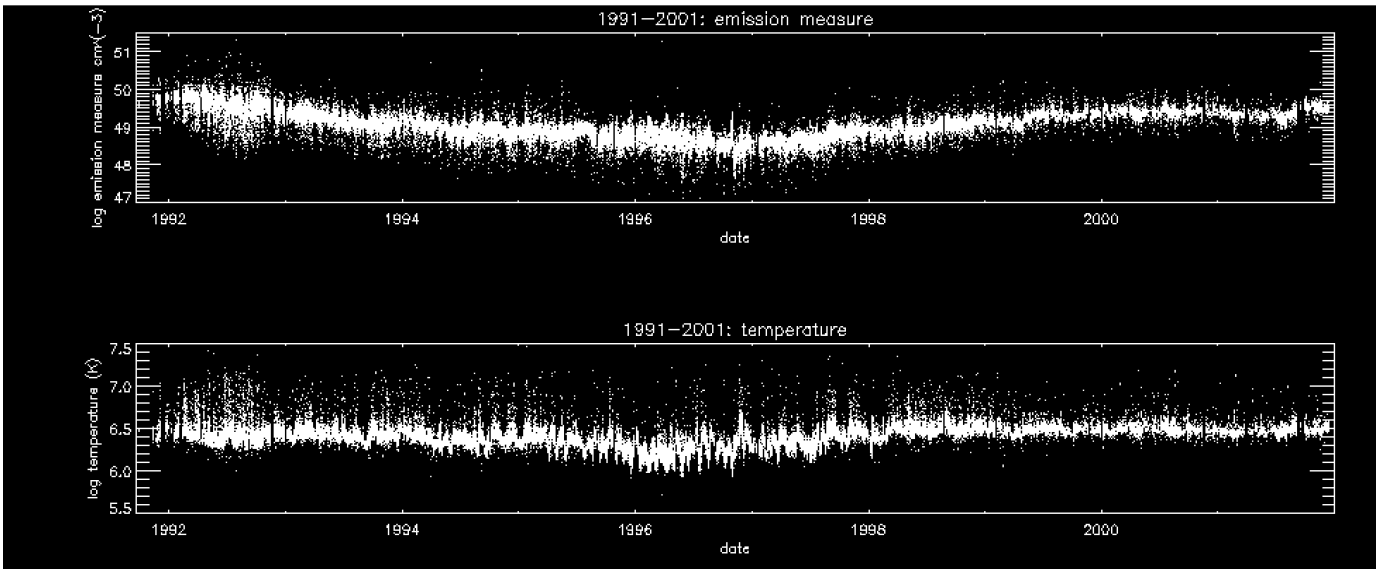

Updated FRM Equation, years 1991-2001, temperature and emission measure. 3-45 Å, 1.2 solar radii. (Graphs should include both old and new FRM equations.)

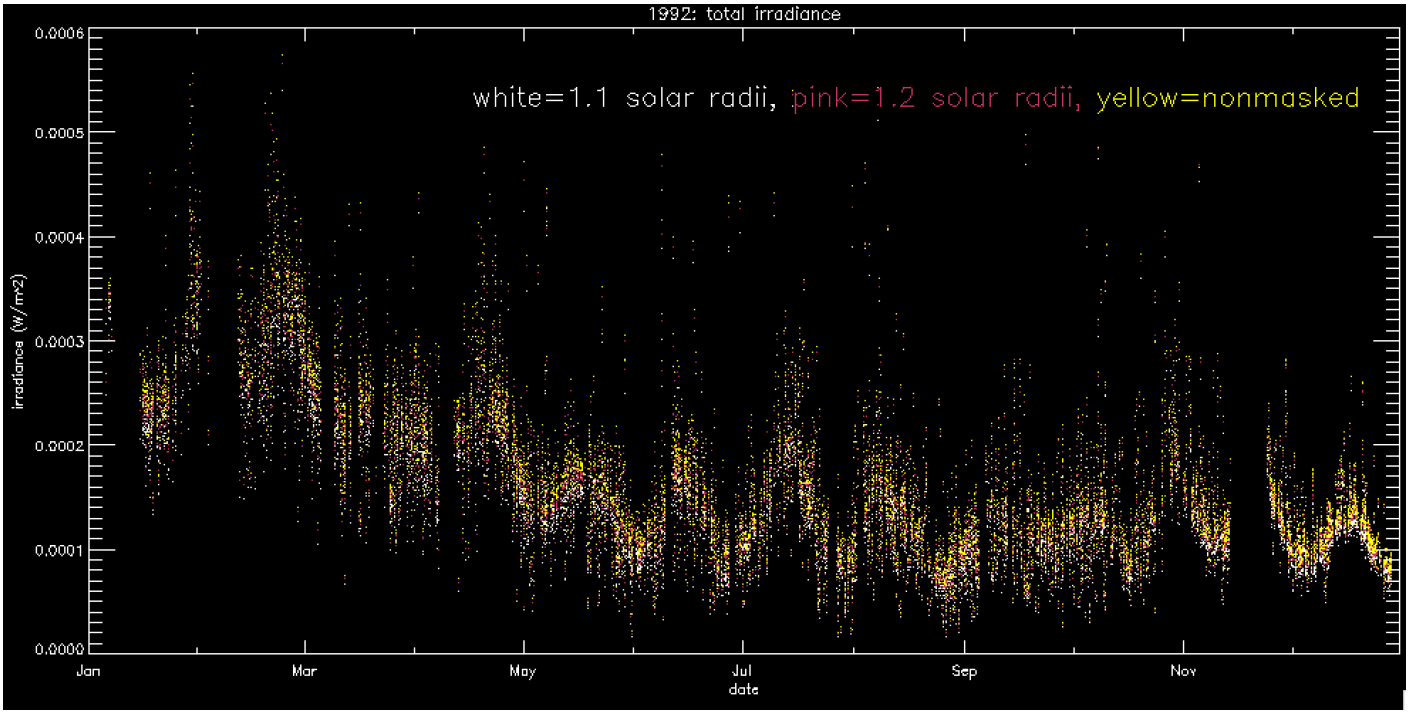

Figure 3. The graph shows the effects on 1992 total irradiance by different masks. Yellow shows the total irradiance of the full picture, white shows the total irradiance of 1.1 solar radii, and the pink shows the total irradiance of 1.2 radii. The white, or data from the full picture, is problematic because the photos are not consistently cropped and many photos have unreliable data. 1.1 radii resulted in a loss of important information. 1.2 radii was chosen for subsequent graphs because it followed the trend of 1.1 radii but included irradiance from coronal mass ejections and other solar activity.

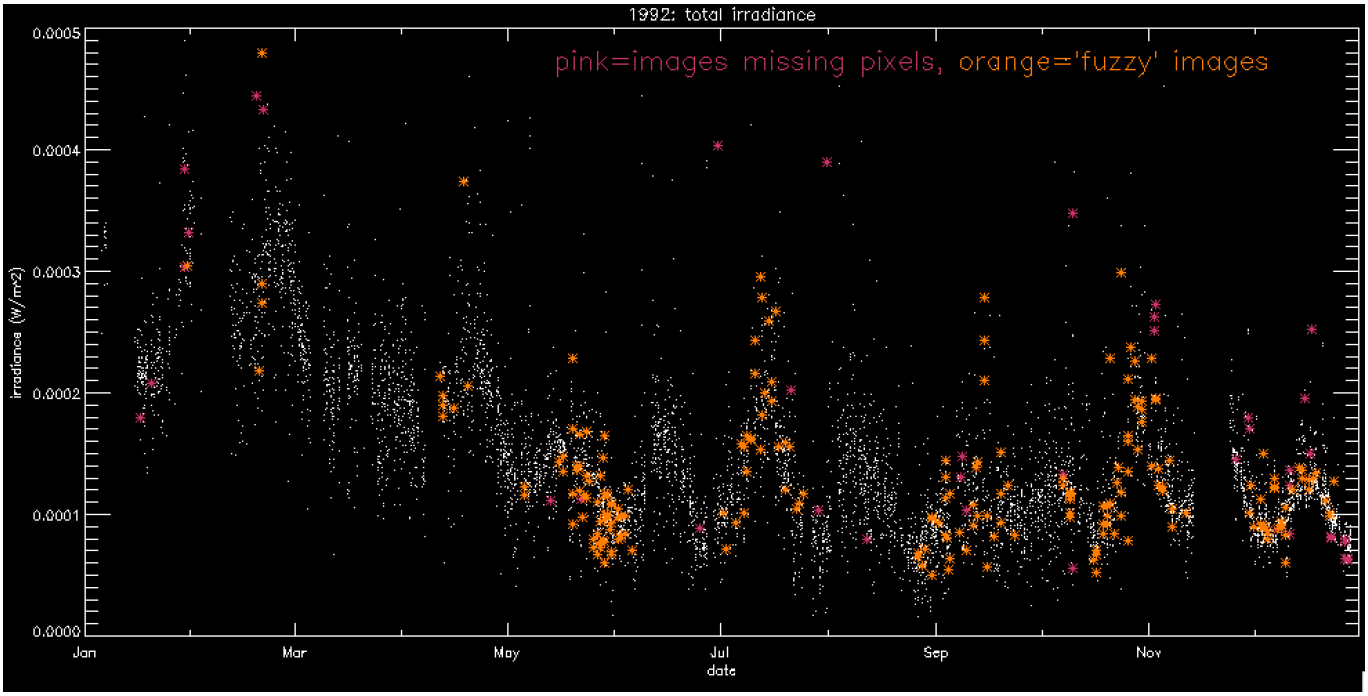

Figure 4. Each picture was analyzed and images with extra cosmic radiation or missing data were marked as unreliable. These images do not seem to have a significant impact on the general trend of total irradiance. However, it is important to note these images when creating a temperature and emission map for each picture with pixel-by-pixel analysis. This takes advantage of Yohkoh's capabilities because its instruments collect more information than a full sun detector could.

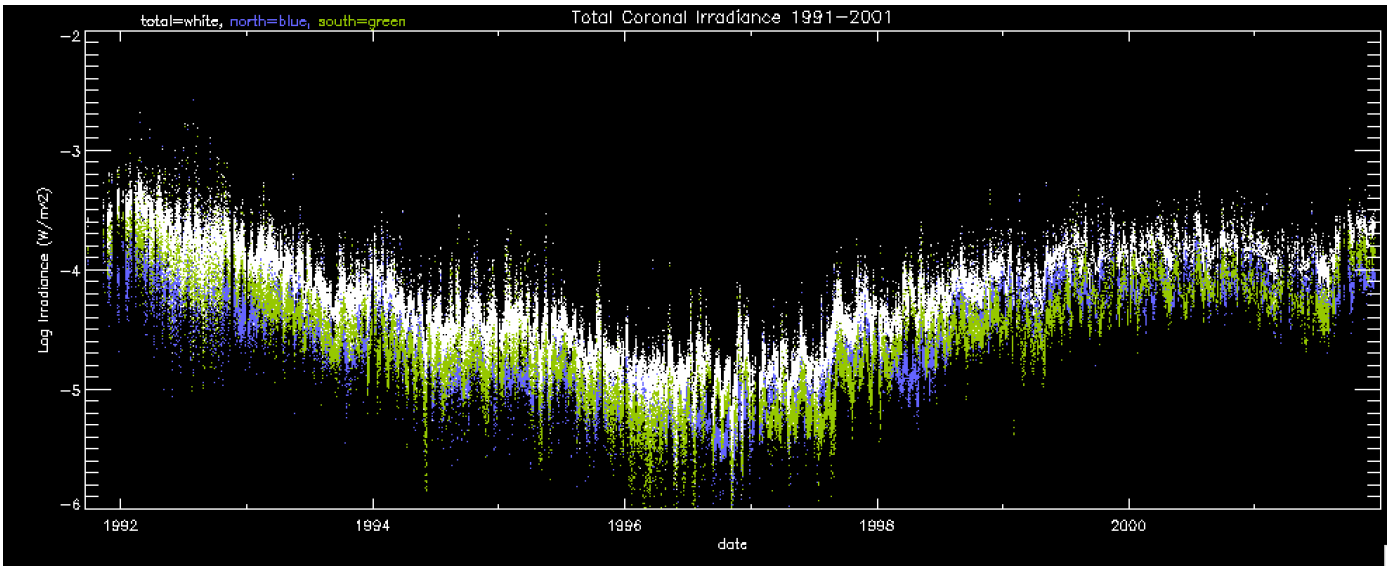

Figure 5. This graph also takes advantage of Yohkoh SXT capabilities by showing a hemispherical breakup of total coronal irradiance from 1991 to

2001. White is the total irradiance, blue is the irradiance of the northern hemisphere, and green is the irradiance of the southern hemisphere.

2. Analysis

The following graphs might be useful for the Analysis section of the paper. Let me know if you would like more information.

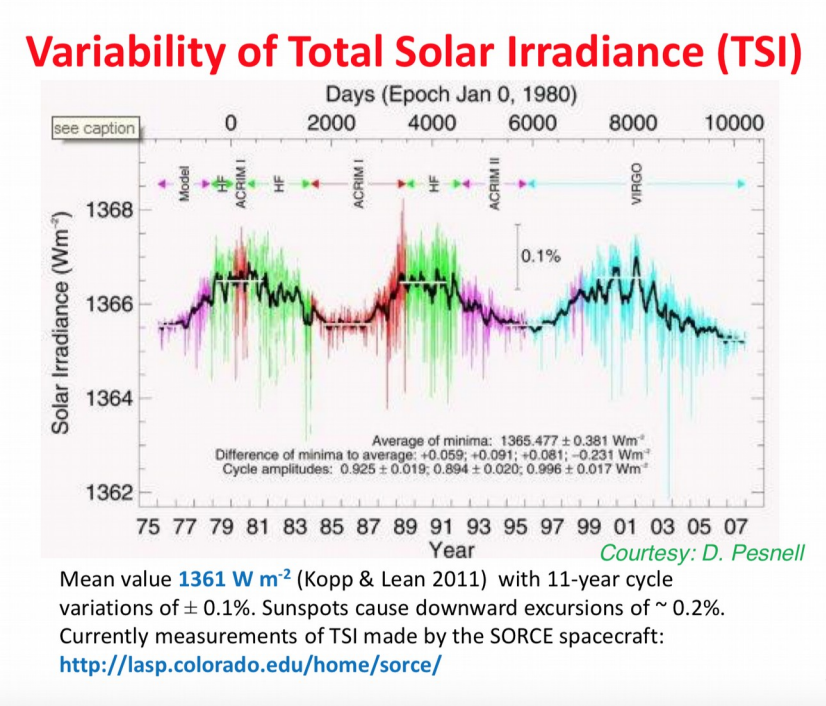

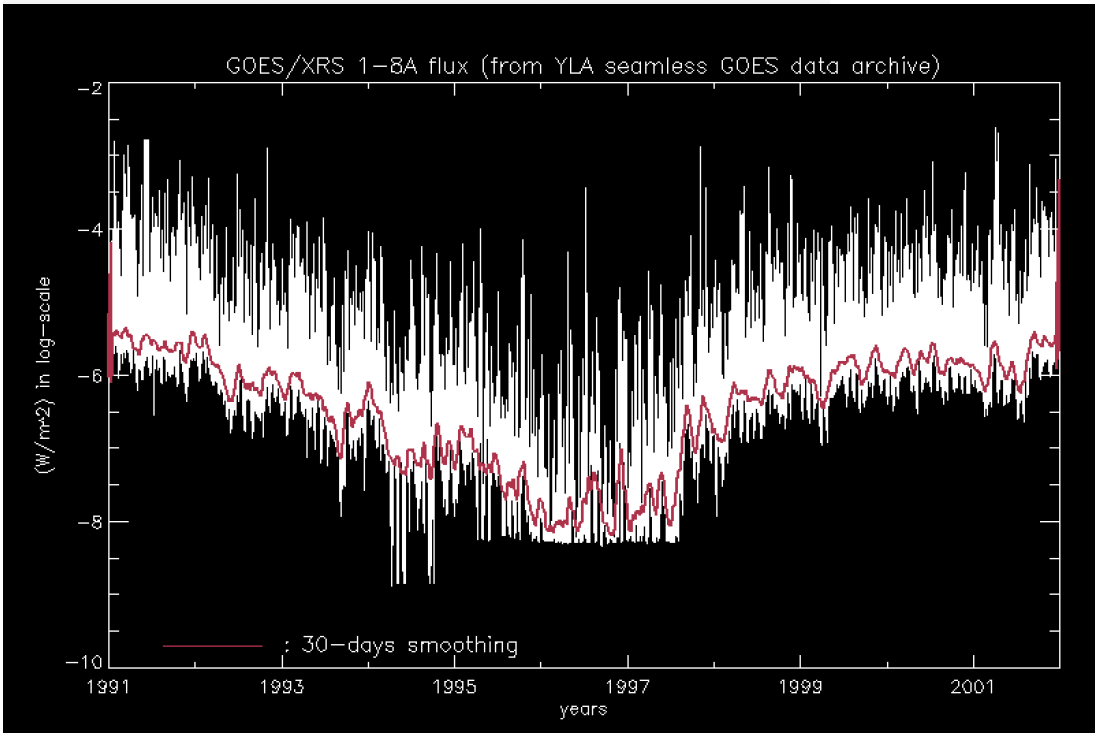

References

"Data Description." *Yohkoh Legacy Data Archive*, Montana State University, 2 Nov. 2010, ylstone.physics.montana.edu/ylegacy/.

Dere, K. P., Landi, E., Mason, H. E., Fossi, B. C., & Young, P. R. (1997, October 15). CHIANTI - an atomic database for emission lines - I. Wavelengths greater than 50 Å. Retrieved from https://aas.aanda.org/articles/aas/abs/1997/13/ds1260/ds1260.html

Garner, R. (2008, January 01). Solar Irradiance. Retrieved December 05, 2018, from https://www.nasa.gov/mission_pages/sdo/science/solar-irradiance.html

Hara et al. (1992) PASJ, vol 44, L135-140, from http://articles.adsabs.harvard.edu/cgi-bin/nph-iarticle_query?1992PASJ...44L.135H&data_type=PDF_HIGH&whole_paper=YES&type=PRINTER&filetype=.pdf

Satellite Drag. (n.d.). Retrieved November 25, 2018, from https://www.swpc.noaa.gov/impacts/satellite-drag

Lang, K. R. (2001). *The Cambridge encyclopedia of the sun*. Cambridge: Cambridge University Press.